Deep Variational Free Energy Calculation of Hydrogen Hugoniot

Zihang Li,[1,2] Hao Xie,[1,3,*] Xinyang Dong,[1,†] and Lei Wang[1,‡]
[1]Beijing National Laboratory for Condensed Matter Physics and Institute of Physics, Chinese Academy of Sciences, Beijing 100190, China
[2]University of Chinese Academy of Sciences, Beijing 100049, China
[3]Department of Astrophysics, University of Zürich, Winterthurerstrasse 190, 8057 Zürich, Switzerland

(Received 30 July 2025; revised 22 December 2025; accepted 20 January 2026; published 20 February 2026)

We develop a deep variational free energy framework to compute the equation of state of hydrogen in the warm dense matter region. This method parameterizes the variational density matrix of hydrogen nuclei and electrons at finite temperature using three deep generative models: a normalizing flow model for the Boltzmann distribution of the classical nuclei, an autoregressive transformer for the distribution of electrons in excited states, and a permutational equivariant flow model for the unitary backflow transformation of electron coordinates in Hartree-Fock states. By jointly optimizing the three neural networks to minimize the variational free energy, we obtain the equation of state and related thermodynamic properties of dense hydrogen for the temperature range where electrons occupy excited states. We compare our results with other theoretical and experimental results on the deuterium Hugoniot curve, aiming to resolve existing discrepancies. Our results bridge the gap between the results obtained by path-integral Monte Carlo calculations at high temperature and ground-state electronic methods at low temperature, thus providing a valuable benchmark for hydrogen in the warm dense matter region.

DOI: 10.1103/8zn5-6dnt

Introduction—Hydrogen is the most abundant element in the universe. A full understanding of the hydrogen phase diagram under extreme conditions [1,2] is important for many applications ranging from planetary science [3–6] to inertial confinement fusion [7–9]. In particular, in the warm dense matter (WDM) region [10–14], hydrogen undergoes the molecular-to-atomic transition [15,16], approaches metallization [17], and exhibits a delicate interplay of quantum and thermal effects in dense plasmas [18,19]. A thorough understanding of this regime is crucial for accurately modeling hydrogen-rich giant planets (such as Jupiter), and for optimizing inertial-confinement-fusion implosions, whose efficiency hinges on the chosen compression pathway.

The Hugoniot curve [20], obtained by tracing the locus of shock-compressed states during dynamic loading of hydrogen, offers a crucial experimental benchmark for constraining hydrogen's equation of state (EOS) in the WDM region. Experimental studies commonly focus on the deuterium Hugoniot curve because deuterium's higher mass density facilitates both the attainment and accurate diagnosis of extreme shock-compressed states [1]. Landmark experiments using gas guns [21–24], lasers [25–34], explosions [35–38], and pulsed power facilities [39–44] have measured the deuterium Hugoniot up to megabar pressures, revealing anomalies such as unexpectedly high compressibility near 50 GPa. These results have not been fully agreed upon [2,45], and have sparked debates over dissociation mechanisms and electronic structure changes, yet experimental data remain sparse at higher temperatures due to diagnostic challenges.

Complementary theoretical approaches have been employed to tackle the deuterium Hugoniot curve challenge, including path-integral Monte Carlo (PIMC) [46–53], coupled electron-ion Monte Carlo (CEIMC) [54,55], density functional theory (DFT) [56–64], machine learning based methods [65,66], and various alternative techniques [18,67–72]. Databases such as SESAME [3] and FPEOS [73] compile EOS data generated by different methods, providing standardized references for both experimental and computational studies. Nevertheless, these collective efforts remain insufficient. For example, restricted PIMC (RPIMC) may suffer from uncontrolled fixed-node error at low temperatures and high density [47], while CEIMC treats electrons in the ground state, thus may become unreliable at finite temperatures [54,55]. To date, there is still a lack of reliable quantum many-body calculations that can provide consistent predictions across the whole temperature range of the Hugoniot curve. Within the framework of quantum many-body methods, the handshake between finite-temperature and ground-state electronic calculations along the Hugoniot curve remains to be established.

*Contact author: qwexiehao@gmail.com
†Contact author: dongxy@iphy.ac.cn
‡Contact author: wanglei@iphy.ac.cn

In this Letter, we combine the deep variational free energy method [74,75], previously applied to ground-state dense hydrogen, with the neural canonical transformation approach [76,77] to compute the excited-state deuterium equation of state and its Hugoniot curve in the temperature regime where electrons occupy excited states, in order to achieve the handshake for the deuterium Hugoniot curve from the finite-temperature side. This regime is particularly challenging for existing methods: ground-state approaches become unreliable when thermal electron excitations are significant, while PIMC methods encounter the fermion sign problem at lower temperatures. We aim to elucidate the phase behavior and provide a reliable EOS for deuterium to serve as a benchmark for future shock experiments and astrophysical modeling. The source code, raw data, and network checkpoints are openly available in the GitHub repositories [78,79] and HuggingFace repository [80].

Method—Consider a system of N deuterium atoms in a periodic cubic cell of side length $L = (4\pi N/3)^{1/3} r_s a_0$, where r_s is the dimensionless Wigner-Seitz parameter and a_0 is the Bohr radius; the Hamiltonian reads,

$$\mathcal{H} = -\frac{1}{2}\sum_{i=1}^{N}\nabla_i^2 + \sum_{I<J}^{N}\frac{1}{|\boldsymbol{s}_I - \boldsymbol{s}_J|} - \sum_{i,I=1}^{N}\frac{1}{|\boldsymbol{r}_i - \boldsymbol{s}_I|} + \sum_{i<j}^{N}\frac{1}{|\boldsymbol{r}_i - \boldsymbol{r}_j|}, \tag{1}$$

where $\boldsymbol{s} \equiv \{\boldsymbol{s}_1, \ldots, \boldsymbol{s}_N\}$ and $\boldsymbol{r} \equiv \{\boldsymbol{r}_1, \ldots, \boldsymbol{r}_N\}$ denote the coordinates of the nuclei and electrons, respectively. Within the temperature range relevant to deuterium Hugoniot experiments (approximately 10^3–10^5 K), the nuclei can be treated as classical particles. Therefore, whether the nuclei are protons or deuterons only affects the entropy of classical nuclei [74]. We focus on deuterium in the following discussion to benchmark with experimental and other computational results. The electrons need to be treated as quantum degenerate at finite temperature since the temperature remains below their Fermi temperature ($\sim 10^5$ K), but a nonnegligible fraction would occupy excited states when the temperature exceeds 10^4 K [55]. To properly account for the finite-temperature effects on both nuclei and electrons, we search for variational density matrix of the following form:

$$\rho = \int d\boldsymbol{s}\, p(\boldsymbol{s}) \sum_{\boldsymbol{k}} p(\boldsymbol{k}|\boldsymbol{s}) |\boldsymbol{s}, \Psi_{\boldsymbol{s},\boldsymbol{k}}\rangle\langle \boldsymbol{s}, \Psi_{\boldsymbol{s},\boldsymbol{k}}|. \tag{2}$$

In Eq. (2), $p(\boldsymbol{s})$ represents the nuclear Boltzmann distribution, and the index $\boldsymbol{k}$ is used to label the (in principle complete) set of electronic basis states under given nuclear coordinates $\boldsymbol{s}$. $p(\boldsymbol{k}|\boldsymbol{s})$ represents the electronic excitation distribution in these states and $\Psi_{\boldsymbol{s},\boldsymbol{k}}(\boldsymbol{r})$ are the corresponding wave functions. The variational free energy $F[\rho] = (1/\beta)\mathrm{Tr}(\rho \ln \rho) + \mathrm{Tr}(\rho\mathcal{H})$ of the system then reads,

$$F = \mathop{\mathbb{E}}_{\boldsymbol{s}\sim p(\boldsymbol{s})}\left\{\frac{1}{\beta}\ln p(\boldsymbol{s}) + \mathop{\mathbb{E}}_{\boldsymbol{k}\sim p(\boldsymbol{k}|\boldsymbol{s})}\left[\frac{1}{\beta}\ln p(\boldsymbol{k}|\boldsymbol{s}) + \mathop{\mathbb{E}}_{\boldsymbol{r}\sim|\Psi_{\boldsymbol{s},\boldsymbol{k}}(\boldsymbol{r})|^2}\left(\frac{\mathcal{H}\Psi_{\boldsymbol{s},\boldsymbol{k}}(\boldsymbol{r})}{\Psi_{\boldsymbol{s},\boldsymbol{k}}(\boldsymbol{r})}\right)\right]\right\}, \tag{3}$$

where the first two terms are related to the nuclear and electronic entropy, respectively. The last term is the internal energy of the system.

By parametrizing the nuclear Boltzmann distribution $p(\boldsymbol{s})$, electronic excitation distribution $p(\boldsymbol{k}|\boldsymbol{s})$, and electron wave function $\Psi_{\boldsymbol{s},\boldsymbol{k}}(\boldsymbol{r})$ by three generative models, one can then minimize Eq. (3) to obtain thermodynamic properties of the system. All three generative models employed in this calculation have tractable normalization factors, which is crucial for estimating the entropy term in the variational free energy. A major difference between Eq. (3) and the ground-state variational free energy expression employed in Refs. [74,75] is that the present approach incorporates both electronic ground and excited states to account for thermal effects on electrons in the WDM region. The computational graph of the variational free energy method is shown in Fig. 1.

The Boltzmann distribution $p(\boldsymbol{s})$ of the nuclei is represented by a flow model, which involves a bijective map between the real coordinates $\boldsymbol{s}$ and a set of uniformly distributed "collective" coordinates $\boldsymbol{\zeta}$. The corresponding probability density reads,

$$p(\boldsymbol{s}) = \frac{1}{L^{3N}}\left|\det\left(\frac{\partial\boldsymbol{\zeta}}{\partial\boldsymbol{s}}\right)\right|. \tag{4}$$

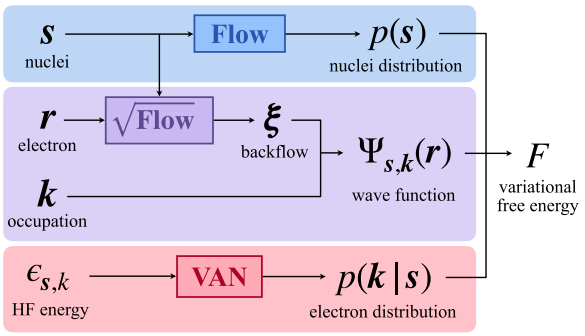

FIG. 1. Computational graph for the finite electron temperature variational free energy calculation. The model consists of three trainable components: a normalizing flow [Eq. (4)] for the nucleus Boltzmann distribution $p(\boldsymbol{s})$ in the blue part; a variational autoregressive network [Eqs. (6), (7a), and (7b)] for the electron excitation distribution $p(\boldsymbol{k}|\boldsymbol{s})$ in the red part; and a quantum flow for the electron wave functions $\Psi_{\boldsymbol{s},\boldsymbol{k}}(\boldsymbol{r})$ shown in Eq. (5) in the purple part. We jointly optimize the three neural networks to minimize the variational free energy F in Eq. (3).

To model a complete set of electronic basis states $|\Psi_{s,k}\rangle$ under given nuclear coordinates s, we adopt the idea of neural canonical transformation proposed in Refs. [76,77]. Specifically, we unitarily transform the set of Hartree-Fock (HF) Slater determinant states by applying an s-dependent bijective map $r \leftrightarrow \xi$ to the electron coordinates. The HF states are computed using a batched HF solver on GTH-DZV basis set, which is sufficient for temperatures up to 62 500 K in this Letter. The resulting many-body wave function reads,

$$\Psi_{s,k}(r) = \det\left[\psi_{s,k_i^\uparrow}(\xi_j^\uparrow)\right] \det\left[\psi_{s,k_i^\downarrow}(\xi_j^\downarrow)\right] \left|\det\left(\frac{\partial \xi}{\partial r}\right)\right|^{\frac{1}{2}}. \quad (5)$$

In this context, the state index $k \equiv \{k_1^\uparrow, \ldots, k_{N/2}^\uparrow, k_1^\downarrow, \ldots, k_{N/2}^\downarrow\}$ is naturally labeled by N occupied HF single-particle orbitals $\psi_{s,k_i^\sigma}(\xi_j^\sigma)$, where $\sigma \in \{\uparrow, \downarrow\}$ denotes the electron spin. Equation (5) is similar in spirit to the backflow transformation, and the transformed coordinates ξ can be physically understood as quasiparticles. The difference lies in the additional Jacobian determinant factor in Eq. (5), which, however, is crucial to ensure the orthonormality of the new basis states [76,77,81–84]. Compared to ground-state neural wave functions [74,75,85], the Jastrow factor cannot be added to our wave functions since it would break the orthogonality. We parametrize the two bijective maps $s \leftrightarrow \zeta, r \leftrightarrow \xi$ mentioned above using neural networks similar to the FermiNet architecture [86]. In particular, we employ permutation-equivariant layers to ensure the symmetry (antisymmetry) property of $p(s)$ ($\Psi_{s,k}$) under permutation of nuclei (electrons with the same spin); see Supplemental Material [87] for details (see also Refs. [88–98] therein).

The electron distribution $p(k|s)$ on the single-particle orbitals is modeled using a masked variational autoregressive network (VAN) [77,99]. For a given nuclear configuration s, the HF solver provides M orthonormal single-particle orbitals $\{\psi_{s,k} | 1 \le k \le M\}$ with corresponding energy levels $\{\epsilon_{s,k} | 1 \le k \le M\}$. The occupation of these orbitals by $N/2$ spin-up and $N/2$ spin-down electrons must satisfy the Pauli exclusion principle. As a result, the distribution $p(k|s)$ factorizes into two components for the spin-up and spin-down sectors

$$p(k|s) = p(k^\uparrow|s)\, p(k^\downarrow|k^\uparrow, s). \quad (6)$$

We employ a mask in VAN to enforce an ordering in which electrons occupy orbitals from lowest to highest energy, i.e., $1 \le k_1^\sigma < k_2^\sigma < \cdots < k_{N/2}^\sigma \le M$. The corresponding probability is expressed as a product of conditional probabilities

$$p(k^\uparrow|s) = \prod_{i=1}^{N/2} p(k_i^\uparrow | k_1^\uparrow, \ldots, k_{i-1}^\uparrow, s), \quad (7a)$$

$$p(k^\downarrow|k^\uparrow, s) = \prod_{i=1}^{N/2} p(k_i^\downarrow | k_1^\downarrow, \ldots, k_{i-1}^\downarrow, k^\uparrow, s). \quad (7b)$$

In order to feed the information of nuclear configuration s into the autoregressive model, we give the analytical conditional probability of noninteracting fermions on HF energy levels into the logit bias of VAN. This makes VAN start with the noninteracting electron distribution, and then learn the interaction effects via the following training. This step is an efficient alternative to the pretraining step in Ref. [77]. See Supplemental Material [87] for details of the masked autoregressive model.

The training curve of the variational free energy method is shown in Fig. 2. The starting point of the training curve is the pretrained flow model based on the HF potential energy surface, combined with the untrained VAN and electron backflow network. The pretraining process is discussed in Supplemental Material [87]. During the training process, the three neural networks are jointly optimized to minimize the free energy defined in Eq. (3) via stochastic optimization. At each optimization step, nucleus and electron configurations are sampled via Monte Carlo sampling from the distributions $p(s)$ and $|\Psi_{s,k}(r)|^2$, while the energy level configurations k are drawn from $p(k|s)$ via direct sampling. The variational free energy is then estimated by computing the expectation values over these samples, as specified in Eq. (3), and the network parameters are updated via stochastic reconfiguration [100]. Due to the variational principle, the approximation becomes closer to the ground truth as the free energy is minimized. To obtain the equation of state of deuterium, we perform variational free energy optimization under different densities and temperatures.

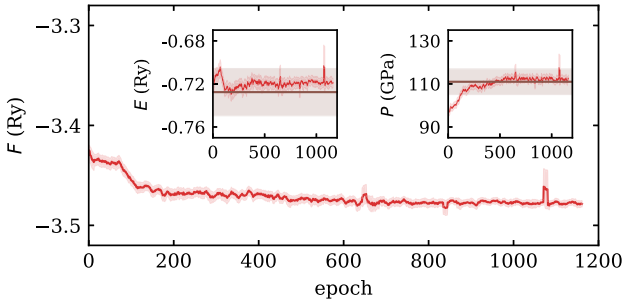

FIG. 2. Training curve of variational free energy method for $N = 32$, $T = 31\,250$ K, $r_s = 2$ deuterium system, with a 10-epoch moving average. The red line in the main figure shows the variational free energy F per atom and the error bar (red-filled area) during training. The red lines in the set insets show the internal energy E per atom and the pressure P change. The brown lines are the PBC $N = 32$ results from RPIMC [47], and the filled areas denote the error bars.

TABLE I. The equation of state and Hugoniot results of deuterium system calculated by variational free energy method. N is the number of atoms in the system. T is the temperature in Kelvin unit. E, P, and S_e are the internal energy (in Rydberg unit), pressure (in GPa), and electronic entropy (in k_B unit) per atom, respectively. The subscripts denote the corresponding r_s values. ρ_{Hugoniot}, E_{Hugoniot}, and P_{Hugoniot} are the Hugoniot density (in units of initial density $\rho_0 = 0.171$ g/cm^3), internal energy (in Rydberg unit), and pressure (in GPa), respectively.

		$r_s = 1.86$			$r_s = 2$					
N	T	E	P	S_e	E	P	S_e	$\rho_{\text{Hugoniot}}/\rho_0$	E_{Hugoniot}	P_{Hugoniot}
54	10 000	−0.9669(18)	65.95(71)	0.0220(4)	−0.9675(13)	45.48(49)	0.0271(4)	4.495(15)	−0.9671(12)	57.34(33)
32	10 000	−0.9726(6)	62.85(34)	0.0549(2)	−0.9778(6)	43.03(28)	0.07003(3)	4.5225(90)	−0.9746(4)	55.11(13)
32	15 625	−0.9050(5)	86.27(33)	0.1600(4)	−0.9077(17)	60.54(51)	0.1751(4)	4.4730(64)	−0.9062(8)	74.89(24)
32	31 250	−0.7105(6)	155.12(33)	0.4389(5)	−0.7089(5)	115.50(26)	0.4794(5)	4.3481(36)	−0.7096(4)	132.43(12)
32	62 500	−0.2939(37)	302.0(13)	0.8353(6)	−0.2892(7)	233.89(28)	0.8890(6)	4.2438(23)	−0.2906(12)	255.58(37)

After the optimization has reached convergence, we carry out inference to evaluate various thermodynamic observables such as the entropy of nuclei and electrons, pressure, and internal energy.

Result—To study the EOS of the deuterium system, we perform calculations on systems containing 14, 20, 32, and 54 atoms. All calculations are carried out using twist boundary conditions (TBC), with the Baldereschi point $(1/4, 1/4, 1/4)$ as the mean-value point. We also apply Chiesa's finite-size correction [101,102] to reduce finite-size errors. See Supplemental Material [87] for details. Table I presents results for systems with $N = 32$ and 54 atoms at various r_s and temperatures. As shown in Table I, the electronic entropy is close to zero at 10 000 K, indicating that most electrons remain in the ground state. As the temperature increases, electrons are gradually thermally excited to higher energy levels. We can also see this intuitively in Fig. 3(a), which shows the electron occupation of single-particle orbitals. At 10 000 K, the electron occupation closely resembles that of the ground state (the dashed black line). As temperature rises, electrons increasingly occupy higher energy levels, leading to a broader distribution. This Fermi-Dirac-like distribution of electrons at finite temperature is captured by VAN. The discontinuous jumps in the occupation at certain energy levels arise from the learning of the neural canonical transformation. After the transformation in Eq. (5), the notions of single-particle orbitals and energy levels are no longer well-defined for the many-body wave function. Instead, the VAN determines whether to occupy these transformed orbitals based on their contribution to lowering the system's free energy, irrespective of their original Hartree-Fock energy levels. The entropy and occupation results indicate that thermal effects on electrons must be taken into account when the temperature is above 10 000 K.

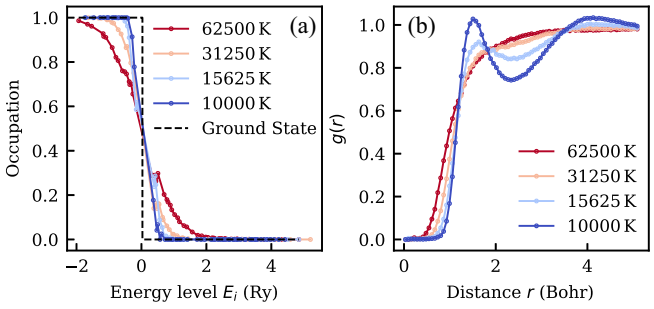

FIG. 3. Electron distribution on single-particle orbitals and nucleus-nucleus RDF of $N = 32$, $r_s = 2$ deuterium system at several temperatures. (a) Electron occupation of single-particle orbitals. E_i are Hartree-Fock energy levels of these orbitals. The dashed black line is ground-state occupation as reference. (b) Nucleus-nucleus RDF.

The nucleus-nucleus radial distribution function (RDF) $g(r)$ is shown in Fig. 3(b). At 62 500 K, $g(r)$ is smooth without any prominent peak, indicating a fully dissociated atomic fluid phase. As the temperature decreases, a peak corresponding to the formation of deuterium molecules gradually emerges. This marks the beginning of the transition from the atomic phase to the molecular phase [65]. The formation of the molecular peak in RDF can be verified by previous variational density matrix calculation [18].

We compute the deuterium Hugoniot curve using the equation of state and the Rankine-Hugoniot relation [103]

$$H = E - E_0 + \frac{1}{2}(P + P_0)(\Omega - \Omega_0) = 0. \tag{8}$$

The reference state used in this Letter is $\rho_0 = 0.171$ g/cm^3, $E_0 = -15.886$ eV, and $P_0 = 0$ GPa, which is the same as that adopted in Ref. [47]. The deuterium Hugoniot curve is typically located in the range $r_s = 1.86$ to $r_s = 2$ for temperatures between 10 000 and 62 500 K. We select four representative temperatures for the calculations. At each temperature, the EOS points are computed at $r_s = 1.86$ and $r_s = 2$. The Hugoniot density and corresponding pressure are then obtained via Lagrange interpolation, as summarized in Table I. The interpolated Hugoniot curve for the $N = 32$ and $N = 54$ deuterium system is shown in Fig. 4. The yellow star denotes the result at 10 000 K for the $N = 54$ system, which corresponds to the regime where

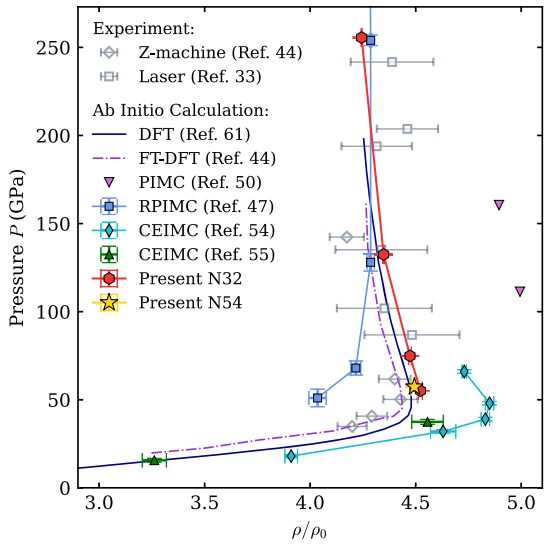

FIG. 4. Pressure-compression ratio diagram of Hugoniot experiments and computations. The red symbols are Lagrange interpolation of variational free energy results of $N = 32$ system, the yellow star is the result at 10 000 K for the $N = 54$ system. The experimental and theoretical results are from Z-machine [44], laser [33], DFT molecular dynamics (DFT) [61], DFT with finite-temperature XC functionals (FT-DFT) [44], direct PIMC [50], RPIMC [47], and CEIMC [54,55].

finite-size effects are expected to be most pronounced, as shell effects are particularly strong at low temperatures. This computationally expensive calculation is included to benchmark the magnitude of finite-size effects in our Letter. Our results are consistent with the available experimental data [33,44]. As shown in Fig. 4, at low temperatures, our Hugoniot compression ratio ρ/ρ_0 is slightly higher than the DFT results, significantly higher than those from RPIMC [47], and substantially lower than the CEIMC results [54]. With increasing temperature, our results show good agreement with RPIMC. It should be noted that the PIMC method suffers from the fermion sign problem [104,105] at low temperatures and small r_s, where electron-electron interactions become strong. Moreover, the RPIMC method relies on the fixed-node approximation, which can introduce systematic errors and requires additional effort to determine appropriate nodal surfaces. In contrast, the variational free energy method employed here is free from the fermion sign problem and does not impose any restricted approximations on the electronic degrees of freedom. The computational procedure remains the same across different temperatures and values of r_s.

Conclusion—In this Letter, we further develop the variational free energy method using three generative neural networks to parameterize the density matrix of the warm dense deuterium system. By optimizing the variational free energy with respect to three neural networks, we calculate the EOS and Hugoniot curve of deuterium within the temperature range where electrons are slightly excited (10 000–62 500 K). We focus on this temperature regime to bridge the gap from the finite-temperature side, as existing ground-state methods become unreliable when thermal electron excitations are significant, while PIMC methods suffer from the fermion sign problem at lower temperatures. The advantage of the variational free energy method compared to PIMC is that there is no exponential computational complexity caused by the fermion sign problem, and it can directly compute entropy and free energy. Compared to CEIMC, the variational free energy method effectively accounts for finite-temperature effects on electrons, which is critical for studying WDM. Moreover, the variational principle ensures its reliability. The resulting Hugoniot curve, computed with TBC and analytical finite-size corrections for systems up to 54 atoms, shows good agreement with experimental measurements, connects smoothly with PIMC results at high temperatures, and extends into the low-temperature regime where PIMC suffers from the fermion sign problem, thereby achieving the handshake between ground-state and finite-temperature calculations from the finite-temperature side. In conclusion, our results provide the EOS and Hugoniot curve of deuterium for benchmarking future experiments and theoretical methods. We note that recent advances in PIMC methods [106–113] may further verify our results.

Acknowledgments—We are grateful for the useful discussions with Xinguo Ren, Mohan Chen, Garnet Chan, Shiwei Zhang, Markus Holzmann, Michele Casula, Qi Zhang, Zhendong Cao, Xingyu Zhang, Qi Yang, Ruisi Wang, Zongguo Wang, Chunbao Zhou, Qinmeng Yang, Jiaheng Wang, and Lei Tang. This work is supported by the Strategic Priority Research Program of the Chinese Academy of Sciences under Grant No. XDB0500000; the National Natural Science Foundation of China under Grants No. 92270107, No. T2225018, No. 12188101, No. T2121001, and No. 12504289; and the National Key Projects for Research and Development of China Grant No. 2021YFA1400400.

Data availability—The data that support the findings of this article are openly available [78–80].

[1] J. M. McMahon, M. A. Morales, C. Pierleoni, and D. M. Ceperley, Rev. Mod. Phys. **84**, 1607 (2012).
[2] M. Bonitz, J. Vorberger, M. Bethkenhagen, M. P. Böhme, D. M. Ceperley, A. Filinov, T. Gawne, F. Graziani, G. Gregori, P. Hamann *et al.*, Phys. Plasmas **31**, 110501 (2024).
[3] G. I. Kerley, Phys. Earth Planet. Inter. **6**, 78 (1972).
[4] B. Militzer, W. B. Hubbard, J. Vorberger, I. Tamblyn, and S. A. Bonev, Astrophys. J. **688**, L45 (2008).
[5] I. Baraffe, G. Chabrier, and T. Barman, Rep. Prog. Phys. **73**, 016901 (2009).

[6] Y. Miguel, T. Guillot, and L. Fayon, Astron. Astrophys. **596**, A114 (2016).
[7] J. Lindl, Phys. Plasmas **2**, 3933 (1995).
[8] R. Craxton, K. Anderson, T. Boehly, V. Goncharov, D. Harding, J. Knauer, R. McCrory, P. McKenty, D. Meyerhofer, J. Myatt *et al.*, Phys. Plasmas **22**, 110501 (2015).
[9] S. X. Hu, V. N. Goncharov, T. R. Boehly, R. L. McCrory, S. Skupsky, L. A. Collins, J. D. Kress, and B. Militzer, Phys. Plasmas **22**, 056304 (2015).
[10] K. Falk, High Power Laser Sci. Eng. **6**, e59 (2018).
[11] M. Bonitz, T. Dornheim, Z. A. Moldabekov, S. Zhang, P. Hamann, H. Kählert, A. Filinov, K. Ramakrishna, and J. Vorberger, Phys. Plasmas **27**, 042710 (2020).
[12] C. A. Ullrich, A. Pribram-Jones, S. Pittalis, E. K. U. Gross, K. Burke, V. V. Karasiev, T. Sjostrom, D. Chakraborty, J. W. Dufty, K. Runge *et al.*, *Frontiers and Challenges in Warm Dense Matter*, edited by F. Graziani, M. P. Desjarlais, R. Redmer, and S. B. Trickey (Springer, Cham, Switzerland, 2014), Vol. 96.
[13] J. Vorberger, F. Graziani, D. Riley, A. D. Baczewski, I. Baraffe, M. Bethkenhagen, S. Blouin, M. P. Böhme, M. Bonitz, M. Bussmann *et al.*, arXiv:2505.02494.
[14] M. Böhme, Z. A. Moldabekov, J. Vorberger, and T. Dornheim, Phys. Rev. Lett. **129**, 066402 (2022).
[15] B. Militzer and D. M. Ceperley, Phys. Rev. E **63**, 066404 (2001).
[16] Z. Moldabekov, S. Schwalbe, M. P. Böhme, J. Vorberger, X. Shao, M. Pavanello, F. R. Graziani, and T. Dornheim, J. Chem. Theory Comput. **20**, 68 (2023).
[17] M. D. Knudson, M. P. Desjarlais, A. Becker, R. W. Lemke, K. R. Cochrane, M. E. Savage, D. E. Bliss, T. R. Mattsson, and R. Redmer, Science **348**, 1455 (2015).
[18] B. Militzer and E. L. Pollock, Phys. Rev. E **61**, 3470 (2000).
[19] W. R. Magro, D. M. Ceperley, C. Pierleoni, and B. Bernu, Phys. Rev. Lett. **76**, 1240 (1996).
[20] Y. B. Zel'dovich and Y. P. Raizer, *Physics of Shock Waves and High-Temperature Hydrodynamic Phenomena*, edited by W. D. Hayes and R. F. Probstein (Academic Press, New York, 1967).
[21] R. D. Dick and G. I. Kerley, J. Chem. Phys. **73**, 5264 (1980).
[22] W. J. Nellis, A. C. Mitchell, M. van Thiel, G. J. Devine, R. J. Trainor, and N. Brown, J. Chem. Phys. **79**, 1480 (1983).
[23] W. J. Nellis, M. Ross, A. C. Mitchell, M. van Thiel, D. A. Young, F. H. Ree, and R. J. Trainor, Phys. Rev. A **27**, 608 (1983).
[24] N. C. Holmes, M. Ross, and W. J. Nellis, Phys. Rev. B **52**, 15835 (1995).
[25] L. Da Silva, P. Celliers, G. Collins, K. Budil, N. Holmes, T. Barbee Jr, B. Hammel, J. Kilkenny, R. Wallace, M. Ross *et al.*, Phys. Rev. Lett. **78**, 483 (1997).
[26] G. W. Collins, L. B. D. Silva, P. Celliers, D. M. Gold, M. E. Foord, R. J. Wallace, A. Ng, S. V. Weber, K. S. Budil, and R. Cauble, Science **281**, 1178 (1998).
[27] G. W. Collins, P. M. Celliers, L. B. Da Silva, R. Cauble, D. M. Gold, M. E. Foord, N. C. Holmes, B. A. Hammel, R. J. Wallace, and A. Ng, Phys. Rev. Lett. **87**, 165504 (2001).
[28] M. D. Knudson, D. L. Hanson, J. E. Bailey, C. A. Hall, and J. R. Asay, Phys. Rev. Lett. **90**, 035505 (2003).
[29] T. Boehly, D. Hicks, P. Celliers, T. Collins, R. Earley, J. Eggert, D. Jacobs-Perkins, S. Moon, E. Vianello, D. Meyerhofer *et al.*, Phys. Plasmas **11**, L49 (2004).
[30] D. G. Hicks, T. R. Boehly, P. M. Celliers, J. H. Eggert, S. J. Moon, D. D. Meyerhofer, and G. W. Collins, Phys. Rev. B **79**, 014112 (2009).
[31] M. D. Knudson and M. P. Desjarlais, Phys. Rev. Lett. **103**, 225501 (2009).
[32] T. Sano, N. Ozaki, T. Sakaiya, K. Shigemori, M. Ikoma, T. Kimura, K. Miyanishi, T. Endo, A. Shiroshita, H. Takahashi *et al.*, Phys. Rev. B **83**, 054117 (2011).
[33] A. Fernandez-Pañella, M. Millot, D. Fratanduono, M. Desjarlais, S. Hamel, M. Marshall, D. Erskine, P. Sterne, S. Haan, T. Boehly *et al.*, Phys. Rev. Lett. **122**, 255702 (2019).
[34] Z. He, Q. Zhang, H. Liu, G. Jia, X. Huang, Z. Fang, Z. Xie, J. Ye, H. Shu, J. Dong *et al.*, Phys. Rev. B **103**, 134107 (2021).
[35] S. I. Belov, G. V. Boriskov, A. I. Bykov, R. I. Il'kaev, N. B. Luk'yanov, A. Y. Matveev, O. L. Mikhailova, V. D. Selemir, G. V. Simakov, R. F. Trunin *et al.*, J. Exp. Theor. Phys. Lett. **76**, 433 (2002).
[36] G. V. Boriskov, A. I. Bykov, R. I. Il'kaev, V. D. Selemir, G. V. Simakov, R. F. Trunin, V. D. Urlin, V. E. Fortov, and A. N. Shuikin, Dokl. Phys. **48**, 553 (2003).
[37] S. Grishechkin, S. Gruzdev, V. K. Gryaznov, M. V. Zhernokletov, R. I. Il'kaev, I. Iosilevskii, G. Kashintseva, S. Kirshanov, S. Manachkin, V. B. Mintsev *et al.*, J. Exp. Theor. Phys. Lett. **80**, 398 (2004).
[38] G. V. Boriskov, A. I. Bykov, R. I. Il'kaev, V. D. Selemir, G. V. Simakov, R. F. Trunin, V. D. Urlin, A. N. Shuikin, and W. J. Nellis, Phys. Rev. B **71**, 092104 (2005).
[39] M. K. Matzen, M. Sweeney, R. Adams, J. Asay, J. Bailey, G. Bennett, D. Bliss, D. Bloomquist, T. Brunner, R. e. Campbell *et al.*, Phys. Plasmas **12**, 055503 (2005).
[40] M. D. Knudson, D. L. Hanson, J. E. Bailey, C. A. Hall, J. R. Asay, and W. W. Anderson, Phys. Rev. Lett. **87**, 225501 (2001).
[41] M. D. Knudson, D. L. Hanson, J. E. Bailey, C. A. Hall, J. R. Asay, and C. Deeney, Phys. Rev. B **69**, 144209 (2004).
[42] J. E. Bailey, M. D. Knudson, A. L. Carlson, G. S. Dunham, M. P. Desjarlais, D. L. Hanson, and J. R. Asay, Phys. Rev. B **78**, 144107 (2008).
[43] M. D. Knudson, M. P. Desjarlais, and A. Pribram-Jones, Phys. Rev. B **91**, 224105 (2015).
[44] M. D. Knudson and M. P. Desjarlais, Phys. Rev. Lett. **118**, 035501 (2017).
[45] W. J. Nellis, Phys. Rev. Lett. **89**, 165502 (2002).
[46] B. Militzer, W. Magro, and D. Ceperley, Contrib. Plasma Phys. **39**, 151 (1999).
[47] B. Militzer and D. M. Ceperley, Phys. Rev. Lett. **85**, 1890 (2000).
[48] B. Militzer, D. M. Ceperley, J. D. Kress, J. D. Johnson, L. A. Collins, and S. Mazevet, Phys. Rev. Lett. **87**, 275502 (2001).
[49] V. Bezkrovniy, V. S. Filinov, D. Kremp, M. Bonitz, M. Schlanges, W. D. Kraeft, P. R. Levashov, and V. E. Fortov, Phys. Rev. E **70**, 057401 (2004).

[50] V. S. Filinov, P. R. Levashov, M. Bonitz, and V. E. Fortov, Plasma Phys. Rep. **31**, 700 (2005).
[51] S. X. Hu, B. Militzer, V. N. Goncharov, and S. Skupsky, Phys. Rev. Lett. **104**, 235003 (2010).
[52] S. X. Hu, B. Militzer, V. N. Goncharov, and S. Skupsky, Phys. Rev. B **84**, 224109 (2011).
[53] S. A. Khairallah, J. Shumway, and E. W. Draeger, arXiv: 1108.1711.
[54] N. M. Tubman, E. Liberatore, C. Pierleoni, M. Holzmann, and D. M. Ceperley, Phys. Rev. Lett. **115**, 045301 (2015).
[55] M. Ruggeri, M. Holzmann, D. M. Ceperley, and C. Pierleoni, Phys. Rev. B **102**, 144108 (2020).
[56] T. J. Lenosky, S. R. Bickham, J. D. Kress, and L. A. Collins, Phys. Rev. B **61**, 1 (2000).
[57] M. P. Desjarlais, Phys. Rev. B **68**, 064204 (2003).
[58] S. A. Bonev, B. Militzer, and G. Galli, Phys. Rev. B **69**, 014101 (2004).
[59] B. Holst, R. Redmer, and M. P. Desjarlais, Phys. Rev. B **77**, 184201 (2008).
[60] C. Wang, X.-T. He, and P. Zhang, J. Appl. Phys. **108**, 044909 (2010).
[61] L. Caillabet, S. Mazevet, and P. Loubeyre, Phys. Rev. B **83**, 094101 (2011).
[62] M. A. Morales, L. X. Benedict, D. S. Clark, E. Schwegler, I. Tamblyn, S. A. Bonev, A. A. Correa, and S. W. Haan, High Energy Density Phys. **8**, 5 (2012).
[63] C. Wang and P. Zhang, Phys. Plasmas **20**, 092703 (2013).
[64] V. V. Karasiev, S. X. Hu, M. Zaghoo, and T. R. Boehly, Phys. Rev. B **99**, 214110 (2019).
[65] G. Tenti, K. Nakano, A. Tirelli, S. Sorella, and M. Casula, Phys. Rev. B **110**, L041107 (2024).
[66] J. X. D'Souza, S. X. Hu, D. I. Mihaylov, V. V. Karasiev, V. N. Goncharov, and S. Zhang, Phys. Plasmas **32**, 042701 (2025).
[67] T. J. Lenosky, J. D. Kress, and L. A. Collins, Phys. Rev. B **56**, 5164 (1997).
[68] M. Ross, Phys. Rev. B **58**, 669 (1998).
[69] D. Saumon, G. Chabrier, and H. M. van Horn, Astrophys. J. Suppl. Ser. **99**, 713 (1995).
[70] Y. Lavrinenko, P. R. Levashov, D. V. Minakov, I. V. Morozov, and I. A. Valuev, Phys. Rev. E **104**, 045304 (2021).
[71] M. Knaup, P.-G. Reinhard, C. Toepffer, and G. Zwicknagel, J. Phys. A **36**, 6165 (2003).
[72] H. Juranek and R. Redmer, J. Chem. Phys. **112**, 3780 (2000).
[73] B. Militzer, F. González-Cataldo, S. Zhang, K. P. Driver, and F. m. c. Soubiran, Phys. Rev. E **103**, 013203 (2021).
[74] H. Xie, Z.-H. Li, H. Wang, L. Zhang, and L. Wang, Phys. Rev. Lett. **131**, 126501 (2023).
[75] X. Dong, H. Xie, Y. Chen, W. Liang, L. Zhang, L. Wang, and H. Wang, Phys. Rev. B **111**, 214118 (2025).
[76] H. Xie, L. Zhang, and L. Wang, J. Mach. Learn. Res. **1**, 38 (2022).
[77] H. Xie, L. Zhang, and L. Wang, SciPost Phys. **14**, 154 (2023).
[78] See https://github.com/fermiflow/Hugoniot for source code of variational free energy calculations.
[79] See https://github.com/ZihangL/hqc for source code of the HF solver.
[80] See https://huggingface.co/datasets/Kelvin2025q/hugoniot for raw data and trained model checkpoints.
[81] Q. Zhang, R.-S. Wang, and L. Wang, J. Chem. Phys. **161**, 024103 (2024).
[82] Q. Zhang, X. Wang, R. Shi, X. Ren, H. Wang, and L. Wang, Phys. Rev. Lett. **134**, 246101 (2025).
[83] Q. Zhang and L. Wang, Phys. Rev. B **112**, 174106 (2025).
[84] Y. Saleh, Á. Fernández Corral, E. Vogt, A. Iske, J. Küpper, and A. Yachmenev, J. Chem. Theory Comput. **21**, 5221 (2025).
[85] D. Linteau, S. Moroni, G. Carleo, and M. Holzmann, arXiv:2504.07062.
[86] D. Pfau, J. S. Spencer, A. G. D. G. Matthews, and W. M. C. Foulkes, Phys. Rev. Res. **2**, 033429 (2020).
[87] See Supplemental Material at http://link.aps.org/supplemental/10.1103/8zn5-6dnt for derivation, method detail, and data analysis, which includes Refs. [88–98].
[88] Q. Sun, T. C. Berkelbach, N. S. Blunt, G. H. Booth, S. Guo, Z. Li, J. Liu, J. D. McClain, E. R. Sayfutyarova, S. Sharma *et al.*, WIREs Comput. Mol. Sci. **8**, e1340 (2018).
[89] G. Lippert, J. Hutter, and M. Parrinello, Mol. Phys. **92**, 477 (1997).
[90] S. Alavi, Angew. Chem., Int. Ed. **48**, 9404 (2009).
[91] J. Bradbury, R. Frostig, P. Hawkins, M. J. Johnson, C. Leary, D. Maclaurin, G. Necula, A. Paszke, J. VanderPlas, S. Wanderman-Milne *et al.*, JAX: composable transformations of Python + NumPy programs, (2018), http://github.com/google/jax.
[92] P. Borrmann and G. Franke, J. Chem. Phys. **98**, 2484 (1993).
[93] C.-C. Zhou and W.-S. Dai, J. Stat. Mech. (2018) P023105.
[94] H. Barghathi, J. Yu, and A. Del Maestro, Phys. Rev. Res. **2**, 043206 (2020).
[95] T. Dornheim, M. Bonitz, Z. A. Moldabekov, S. Schwalbe, P. Tolias, and J. Vorberger, Phys. Rev. B **111**, 115149 (2025).
[96] M. Germain, K. Gregor, I. Murray, and H. Larochelle, in *Proceedings of the 32nd International Conference on Machine Learning*, Proceedings of Machine Learning Research Vol. 37, edited by F. Bach and D. Blei (PMLR, Lille, France, 2015), pp. 881–889.
[97] A. van den Oord, N. Kalchbrenner, and K. Kavukcuoglu, in *Proceedings of The 33rd International Conference on Machine Learning*, Proceedings of Machine Learning Research Vol. 48, edited by M. F. Balcan and K. Q. Weinberger (PMLR, New York, USA, 2016), pp. 1747–1756.
[98] A. Vaswani, N. Shazeer, N. Parmar, J. Uszkoreit, L. Jones, A. N. Gomez, L. u. Kaiser, and I. Polosukhin, in *Advances in Neural Information Processing Systems* Vol. 30, edited by I. Guyon, U. V. Luxburg, S. Bengio, H. Wallach, R. Fergus, S. Vishwanathan, and R. Garnett (Curran Associates, Inc., Long Beach, CA, USA, 2017).
[99] D. Wu, L. Wang, and P. Zhang, Phys. Rev. Lett. **122**, 080602 (2019).

[100] F. Becca and S. Sorella, *Quantum Monte Carlo Approaches for Correlated Systems* (Cambridge University Press, Cambridge, England, 2017).
[101] S. Chiesa, D. M. Ceperley, R. M. Martin, and M. Holzmann, Phys. Rev. Lett. **97**, 076404 (2006).
[102] M. A. Morales, C. Pierleoni, and D. M. Ceperley, Phys. Rev. E **81**, 021202 (2010).
[103] G. E. Duvall and R. A. Graham, Rev. Mod. Phys. **49**, 523 (1977).
[104] T. Dornheim, Phys. Rev. E **100**, 023307 (2019).
[105] M. Böhme, Z. A. Moldabekov, J. Vorberger, and T. Dornheim, Phys. Rev. E **107**, 015206 (2023).
[106] Y. Xiong and H. Xiong, J. Chem. Phys. **157**, 094112 (2022).
[107] T. Morresi, G. Garberoglio, H. Xiong, and Y. Xiong, Phys. Rev. B **112**, 155131 (2025)..
[108] T. Dornheim, P. Tolias, S. Groth, Z. A. Moldabekov, J. Vorberger, and B. Hirshberg, J. Chem. Phys. **159**, 164113 (2023).
[109] T. Dornheim, Z. Moldabekov, S. Schwalbe, P. Tolias, and J. Vorberger, arXiv:2502.15288.
[110] T. Dornheim, S. Schwalbe, M. P. Böhme, Z. A. Moldabekov, J. Vorberger, and P. Tolias, J. Chem. Phys. **160**, 164111 (2024).
[111] T. Dornheim, Z. A. Moldabekov, S. Schwalbe, and J. Vorberger, Phys. Rev. B **111**, L041114 (2025).
[112] T. Dornheim, P. Tolias, Z. A. Moldabekov, and J. Vorberger, Phys. Rev. Res. **7**, 023250 (2025).
[113] P. Svensson, F. Kalkavouras, U. H. Acosta, Z. A. Moldabekov, P. Tolias, J. Vorberger, and T. Dornheim, J. Phys. Chem. Lett. **16**, 10639 (2025).